Probing the bulk electronic states of Bi_2Se_3 using nuclear magnetic resonance

Ben-Li Young,[1,*] Zong-Yo Lai,[1] Zhijun Xu,[2] Alina Yang,[2] G. D. Gu,[2] Z.-H. Pan,[2] T. Valla,[2] G. J. Shu,[3] R. Sankar,[3] and F. C. Chou[3,4]
[1]*Department of Electrophysics, National Chiao Tung University, Hsinchu City 30010, Taiwan*
[2]*Condensed Matter Physics and Materials Science Department, Brookhaven National Laboratory, Upton, New York 11973, USA*
[3]*Center for Condensed Matter Sciences, National Taiwan University, Taipei 10617, Taiwan*
[4]*National Synchrotron Radiation Research Center, Hsinchu City 30076, Taiwan*
(Received 6 April 2012; published 21 August 2012)

We report a nuclear magnetic resonance (NMR) study of Bi_2Se_3 single crystals grown by three different methods. All the crystals show nine well-resolved peaks in their ^{209}Bi NMR spectra of the nuclear quadrupolar splitting, albeit with an intensity anomaly. Spectra at different crystal orientations confirm that all the peaks are purely from the nuclear quadrupolar effect, with no other hidden peaks. We identify the short nuclear transverse relaxation time (T_2) effect as the main cause of the intensity anomaly. We also show that the ^{209}Bi signal originates exclusively from bulk, while the contribution from the topological surface states is too weak to be detected by NMR. However, the bulk electronic structure in these single crystals is not the same, as identified by the NMR frequency shift and nuclear spin-lattice relaxation rate ($1/T_1$). The difference is caused by the different structural defect levels. We find that the frequency shift and $1/T_1$ are smaller in samples with fewer defects and a lower carrier concentration. Also, the low-temperature power law of the temperature-dependent $1/T_1$ ($\propto T^{\alpha}$) changes from the Korringa behavior $\alpha = 1$ in a highly degenerate semiconductor (where the electrons obey Fermi statistics) to $\alpha < 1$ in a less degenerate semiconductor (where the electrons obey Boltzmann statistics).

DOI: 10.1103/PhysRevB.86.075137 PACS number(s): 73.20.−r, 76.60.−k

I. INTRODUCTION

Bi_2Se_3 is a semiconductor that belongs to the class of thermoelectric materials, Bi_2X_3 (X = Se, Te), which has been extensively studied due to its huge technological potential.[1] Recently, these Bi-based compounds drew a tremendous attention when their topological-insulator character was revealed by angle-resolved photoemission spectroscopy (ARPES).[2,3] Surfaces of these materials are characterized by the existence of gapless surface states while the bulk shows semiconductor-like energy gap in the bulk. Due to the strong spin-orbit interaction, spins of the surface electrons are locked perpendicularly to their momenta, forming a single Dirac-like cone with a chiral spin structure.[4] These states provide a playground for many striking quantum phenomena, such as the image magnetic monopole induced by a point charge,[5] Majorana fermions,[6] and axions inside a topological magnetic insulator.[7] Unfortunately, the as-grown Bi_2Se_3 crystals are always n-type semiconductors[8] with the nonvanishing bulk charge carriers hindering the most interesting phenomena related to the topological nature of the surface states. Therefore, numerous attempts to lower the concentration of bulk carriers by hole doping have been launched, such as in $(Bi_{2-\delta}Ca_{\delta})Se_3$, $BiTl(S_{1-\delta}Se_{\delta})_2$, and $(Bi_{1-\delta}Mg_{\delta})_2Se_3$.[3,9,10] Although selenium vacancies are believed to result in n-type behavior, the attempts to synthesize a p-type Bi_2Se_3 simply by varying the Bi:Se ratio have never been successful.[9] Bi_2Se_3 has been studied by various techniques, but to the best of our knowledge, nuclear magnetic resonance (NMR) has not been attempted so far. Therefore we were motivated to apply NMR to microscopically probe the electronic structure and to study structural defects in Bi_2Se_3.

We have studied single crystals of Bi_2Se_3 grown by three different methods. All the samples show ^{209}Bi NMR spectra with nuclear quadrupolar splitting and an atypical peak intensity profile. By taking the spectra at different crystal orientations, we confirmed that the ^{209}Bi signal is solely from the same bulk site environment with no other hidden peaks. In other words, the signal from the topological surface state is too weak to be detected by NMR. However, the bulk electronic states in different crystals are not the same, as reflected in the NMR peak frequency shift and nuclear spin-lattice relaxation rate ($1/T_1$). Resistivity and ARPES measurements also show a significant difference in the doping level of their electronic energy bands, in agreement with the NMR results. From the NMR linewidths, we can conclude that the defect concentration in these crystals is not the same, resulting in different amounts of charge carriers. We find that the frequency shift and $1/T_1$ are smaller in samples with fewer defects and a lower carrier concentration. The high-conductivity samples show Korringa behavior $1/T_1 \propto T$ at low temperatures; whereas the low-conductivity samples exhibit the power of 0.7. We also find that Bi_2Se_3 samples are diamagnetic, with a weak temperature dependence at low temperature. This is due to the Pauli paramagnetism, which increases slightly at low temperature, while the orbital diamagnetism does not change with temperature.

II. EXPERIMENT

Our Bi_2Se_3 single crystals were prepared using the following three methods: chemical vapor transport (CVT), traveling solvent zone, and Se self-flux growth. In the following discussion, the crystals grown by these three methods are labeled as samples Nos. 1, 2, and 3, respectively. The CVT growth has been achieved using NH_4Cl as a transport agent. The stoichiometric mixture of powder 2Bi + 3Se (1 g) and the NH_4Cl (60 mg) were sealed in an evacuated quartz tube (300 mm × 11 mm). After initial heating at 600 °C for 1 day, the subsequent growth was achieved in a two-zone furnace with

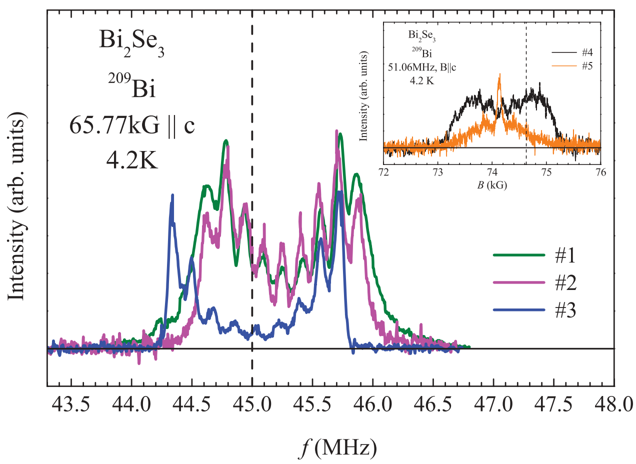

FIG. 1. (Color online) ^{209}Bi NMR frequency-swept spectra in three Bi_2Se_3 single crystals Nos. 1–3 at 4.2 K for a magnetic field of 65.77 kG applied along the c axis. The dashed line denotes the position of the unshifted Larmor frequency $f_0(\mathrm{MHz}) = (\gamma/2\pi)65.77$, where $\gamma/2\pi = 0.684$ MHz/kG is the ^{209}Bi nuclear gyromagnetic ratio. (Inset) ^{209}Bi field-swept spectra of our early Bi_2Se_3 crystals Nos. 4 and 5 (by the Bridgeman[12] and CVT methods, respectively), where the broad linewidth suggests their low quality.

a thermal gradient maintained at 600–500 °C within 30 cm for about a week. Sample No. 2 was grown by a modified floating zone method, where the Se-rich $BiSe_3$ was used in the melting zone. The Bi_2Se_3 material, of high-purity (99.9999%) Bi and Se, was premelted and loaded into a 10-mm diameter quartz tube. The crystal growth rate was controlled at 0.5 mm per hour. Sample No. 3 was prepared by the Se self-flux growth method, using a flux of 3%Bi + 97%Se. The high-purity (99.9999%) Bi and Se were sealed in a 10-mm diameter evacuated quartz tube, heated up to 800 °C, and then cooled down to 250 °C at a cooling rate of 2 °C per hour. At 250 °C, the Bi_2Se_3 single crystals and Se flux were separated in the quartz tube. They then were cooled down to room temperature at a cooling rate of 20 °C per hour.

Note that we measured several Bi_2Se_3 crystals, some from the same batch and some from different batches, after we realized that the NMR results are sample dependent. Our NMR results for these crystals are repeatable. All crystals from one batch generally are of the same quality. Our resistivity, magnetization, and NMR measurements were all on the same piece, and the ARPES was measured in a crystal from the same batch.

The magnetization was measured at 1 kOe for magnetic field applied along the c axis using a Quantum Design superconducting quantum interference device (SQUID). The standard pulsed NMR technique with the spin-echo signals processed using the frequency-shifted-and-summed Fourier transform method was employed throughout our ^{209}Bi NMR spectra.[11] Saturation pulses were used in the $1/T_1$ experiments. The ARPES experiments were carried out at the U13UB beamline of the National Synchrotron Light Source with 18.5 eV photons. The electron analyzer was a Scienta SES-2002 with the combined energy resolution of 8 meV and the angular resolution of ~0.15°. Samples were cleaved *in situ* and measured at ~15 K in the UHV chamber with base pressure 3×10^{-9} Pa.

III. RESULTS AND DISCUSSION

Figure 1 shows the ^{209}Bi NMR frequency-swept spectra of three Bi_2Se_3 samples, for a magnetic field (65.77 kG) applied along the crystalline c axis at a temperature of 4.2 K. The line profiles for samples Nos. 1 and 2 are similar, but different for sample No. 3. However, they all have nine well-resolved and evenly-spaced peaks with lower intensities near the center, confirming the high quality of our crystals. For comparison, the spectra (shown in the inset) of our early low-quality crystals, by the Bridgeman and CVT methods, are relatively broad. At a first glance, these nine sharp peaks appear to depict a nuclear quadrupolar multiplet of the ^{209}Bi sites with a nonzero electric field gradient (EFG), since the nuclear spin of ^{209}Bi is 9/2. However, the peak intensity profile does not resemble the typical nuclear quadrupolar spectrum with the highest intensity central peak and weaker satellites. The intensity profile could be distorted due to additional peaks hiding beneath the quadrupolar satellites. However, according to the Bi_2Se_3 crystal structure, all the bismuth sites are equivalent and it is unlikely for ^{209}Bi to experience different bulk environments.[13] We have ruled out a possibility of hidden peaks, including the contribution from the surface, by measuring the spectra in magnetic field applied along different crystalline directions, as shown in Fig. 2. We find that all the peaks show an angular dependence of the NMR quadrupolar $m \leftrightarrow (m-1)$ level

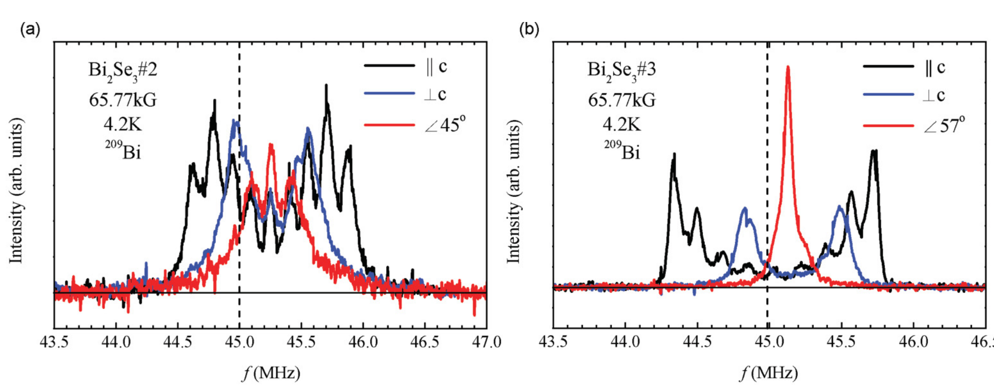

FIG. 2. (Color online) ^{209}Bi NMR frequency-swept spectra of Bi_2Se_3 for (a) sample No. 2 and (b) sample No. 3, with magnetic fields applied at different angles with respect to the c axis. The dashed line denotes the unshifted Larmor frequency position.

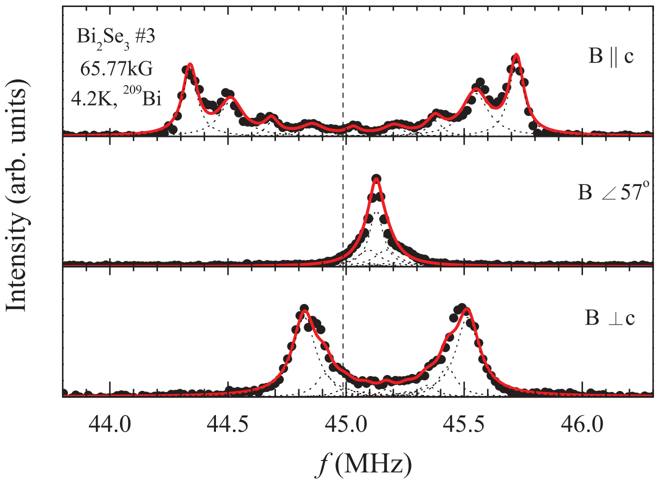

FIG. 3. (Color online) The curve fittings for the ^{209}Bi NMR frequency-swept spectra of Bi_2Se_3, sample No. 3, for the magnetic field directions B$\|$c, B∠57°, and B ⊥ c. (Circles: spectrum points; red curve: fitting curve; dotted curve: individual quadrupolar peaks.)

transition, with the resonance frequency $f_{m\leftrightarrow(m-1)} = (\gamma/2\pi)[1 + K(\theta)]B + f_Q(m - 1/2)(3\cos^2\theta - 1)/2$, where γ is nuclear gyromagnetic ratio of ^{209}Bi, K is the NMR frequency shift, B is the applied magnetic field, f_Q is the nuclear quadrupolar frequency, and θ is the angle of the magnetic field relative to the c axis.[14] We can see that the side peaks move toward the center as the field angle approaches the magic angle $\theta = 54.7^\circ$ (i.e., $3\cos^2\theta - 1 = 0$) at which the quadrupolar splitting vanishes. If there were any hidden peaks, then they should have been separated from the quadrupolar peaks at different field angles, because of their different angle dependance. By fitting the B$\|$c spectra in Fig. 2 to the above equation, we obtain $f_Q = 0.15(5)$ MHz and 0.17(3) MHz for the samples Nos. 2 and 3, respectively. These values are unusually small compared to $f_Q = 2.1$ MHz for a pure Bi metal and several MHz for other bismuth compounds.[15,16] We then fixed the quadrupolar parameters and let the frequency shift $K(\theta)$ as a free fit parameter in the curve fittings for B ⊥ c and B∠57°. The selected fit results are shown in Fig. 3 for the sample No. 3.

The intensity anomaly in the spectra can be explained as an effect of the nuclear spin-spin relaxation time (T_2). We find that the peaks near the center have shorter T_2 than the ones further out on both sides, so that the central peaks decay faster than the side peaks. This is demonstrated in Fig. 4, which shows the NMR intensity decay as a function of T_2 delay time, τ (τ is the time interval between the NMR $\pi/2 - \pi$ echo pulses typically used for T_2 relaxation experiments). However, we could not explain the not monotonic decrease in intensity from the outmost satellite to the central peak in samples Nos. 1 and 2 (see Fig. 1). From the relaxation curves at frequencies 45.04, 45.56, and 45.71 MHz, the relaxation rates, T_2^{-1}, are, respectively, estimated to be 0.043, 0.021, and 0.014 μs^{-1} [see Fig. 4(b)], by fitting the peak points of the curves to the relaxation function $M(\tau) = M(\tau = 0)e^{-2\tau/T_2}$. The intensities in Fig. 4 that oscillate with the T_2 delay time

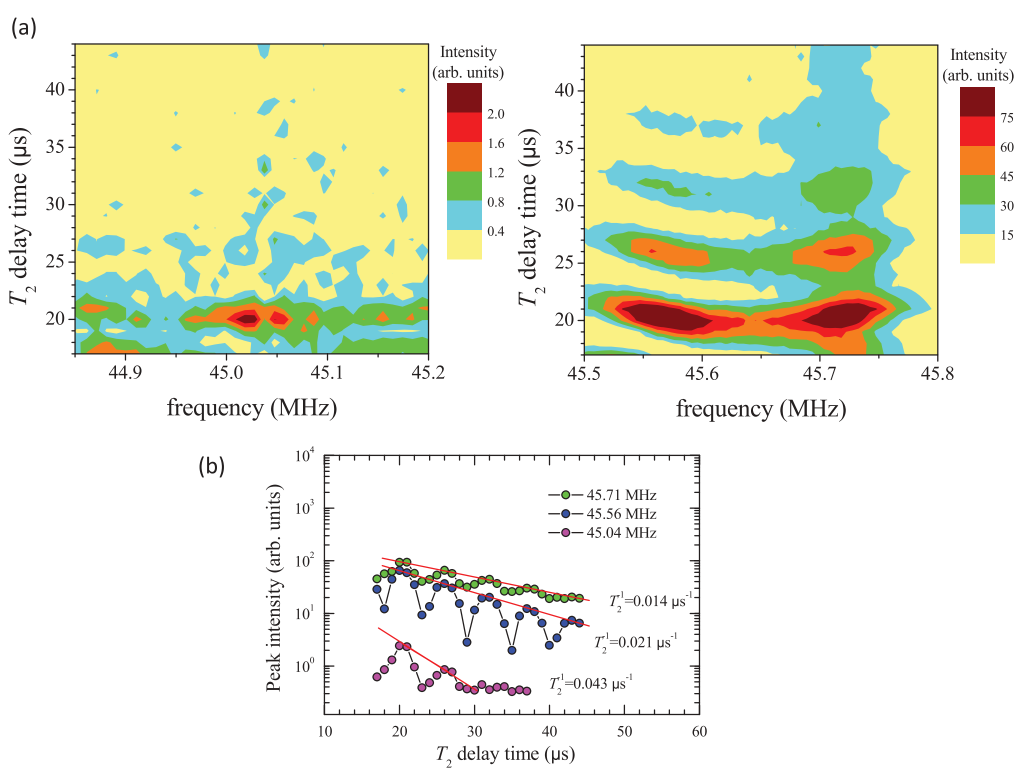

FIG. 4. (Color online) (a) The decay of ^{209}Bi NMR intensity as a function of T_2 delay time (see text) for the Bi_2Se_3 sample No. 3 at 65.77 kG and 4.2 K. The left panel is for peaks near the center. Right panel is for the satellite peaks on the high-frequency side. (b) The T_2 relaxation curves at frequencies 45.04, 45.56, and 45.71 MHz. The red lines are the curve fittings for the points at the peaks of each curve. The relaxation rates T_2^{-1}, obtained from the fits, are labeled next to the curves.

with the period $\tau \sim 6\ \mu$s are a common feature of the nuclear quadrupolar effect.[17] They satisfy the relation $\Delta f_Q \tau \sim 1$, where $\Delta f_Q \sim 0.16$ MHz is the separation of the peaks in Fig. 1. Therefore we have confirmed that the ^{209}Bi NMR signal is coming solely from the same site environment in the bulk of Bi_2Se_3. Given the overwhelming signal from the bulk states within the 200-μm skin depth of the NMR excitation pulses, the ^{209}Bi NMR has insufficient sensitivity for the weak contribution from the topological surface state that is localized to only a few quintuplet layers from the surface. Also, our NMR did not detect the antisite defects for Bi/Se mixing in Bi_2Se_3. Note that the antisite defects tend to occur in Bi_2Te_3.[18]

Figure 1 shows that the NMR frequency shift for the central peak in sample No. 3 is different from those in the other two crystals. Also, the spectral linewidth in that sample is different. These suggest that the electronic states and the structural defect level are different in the studied crystals. The linewidth difference could be qualitatively judged by comparing their outermost satellites. Sample No. 3 has the smallest linewidth because it has the shortest tail. We can infer that the defect concentration is lower in sample No. 3 than in samples Nos. 1 and 2. These defects are mostly due to the Se vacancies that cause the electron doping and a partial occupation of the conduction band.[8] Indeed, the ARPES spectra show a significant difference in the electronic structure between the samples Nos. 2 and 3. Not only is the cone of topological surface state more occupied with electrons, but also, the parabolic bottom of the bulk conduction band is clearly visible in the spectrum of sample No. 2, while it is nearly completely absent from the spectrum of sample No. 3. This indicates that both the bulk and the surface of sample No. 3 have much lower carrier (electron) concentration than the other two samples. This is also reflected in transport, where resistivity of sample No. 3 is an order of magnitude higher than that in sample No. 2 (see Fig. 5).

The NMR frequency shift in Bi_2Se_3 arises from the spin and orbital moments of electrons that interact with nuclei via the hyperfine interactions, such as Fermi contact and dipolar interactions.[19] The Fermi contact interaction gives an isotropic frequency shift due to the *s*-wave conduction electrons in Bi_2Se_3. This shift is expected to be proportional to the electronic density of states. In contrast, the dipole interaction usually produces an anisotropic frequency shift. From Fig. 2, we see that the frequency shift is slightly anisotropic in sample No. 3, but is isotropic in sample No. 2. By analyzing the frequency shifts, $K(\theta)$ (obtained from the previous curve fittings), using the angle-dependent shift, $K(\theta) = K_{\rm iso} + K_{\rm ax}(3\cos^2\theta - 1)$, where $K_{\rm iso}$ and $K_{\rm ax}$ respectively are the isotropic (average) shift and axial shift,[20] we obtained $K_{\rm iso} = 0.65\% \pm 0.05\%$ and $K_{\rm ax} = 0 \pm 0.05\%$ for sample No. 2, and $K_{\rm iso} = 0.34\% \pm 0.05\%$ and $K_{\rm ax} = -0.10\% \pm 0.05\%$ for sample No. 3. Positive $K_{\rm iso}$ suggests that the frequency shift is dominated by the Fermi contact interaction, even though Bi_2Se_3 is diamagnetic.[21] From the magnitude of $K_{\rm iso}$, which is related to the electronic density, we infer that the sample No. 3 has fewer conduction electrons than the sample No. 2. The ARPES results in the insets of Fig. 5 fully support this. While the bottom of bulk conduction band is clearly visible in sample No. 2, it is essentially absent from the spectrum of sample No. 3. Therefore the conduction

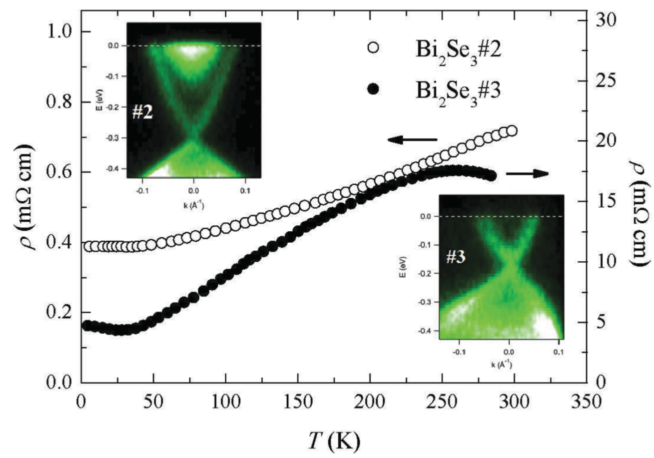

FIG. 5. (Color online) Temperature-dependent resistivity for Bi_2Se_3 samples No. 2 (open circles) and No. 3 (solid circles). The corresponding ARPES spectra (insets) show a significant shift in the chemical potential between these two samples, indicating higher carrier concentration in sample No. 2. The spectra were recorded along the ΓK line in the surface Brillouin zone.

band is shifted above the Fermi level in sample No. 3, at least in the surface region (we note that there might be a slight band bending near the surface). The conelike state, corresponding to the topological surface state, is also shifted upwards relative to the one in sample No. 2. This indicates that the sample No. 3 has less electrons, both in bulk and at the surface. Since the sample No. 2 has more charge carriers, the anisotropic term is overwhelmed by the isotropic term from conduction electrons. The sample No. 3, which has fewer conduction electrons, shows a weak anisotropic shift, an indicative of the dipole interaction.

Figure 6 shows the temperature dependence of the nuclear spin-lattice relaxation rate ($1/T_1$) in the Bi_2Se_3 crystals. The similarity of samples Nos. 1 and 2, as compared to the relatively different sample No. 3, is again reflected in the $1/T_1$ data. The relaxation mechanism for ^{209}Bi $1/T_1$ in Bi_2Se_3 includes the magnetic relaxation ($1/T_{1,\rm m}$) from the scattering

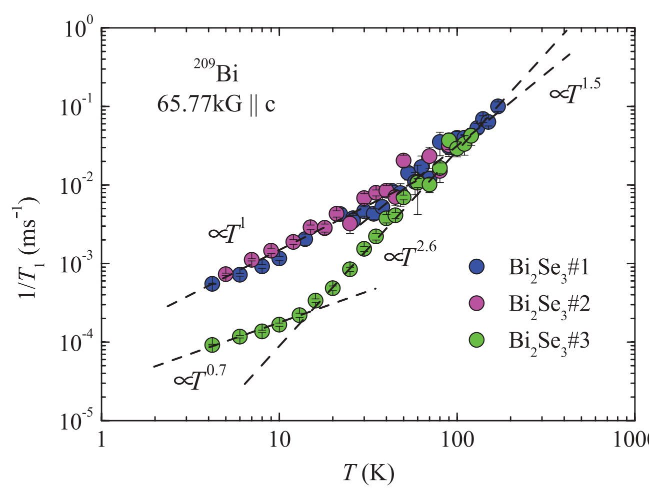

FIG. 6. (Color online) Temperature dependence of nuclear spin-lattice relaxation rate ($1/T_1$) for Bi_2Se_3 crystals.

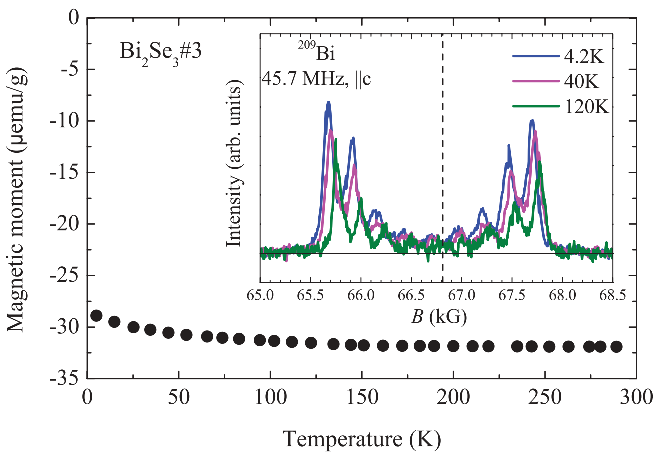

FIG. 7. (Color online) Temperature-dependent magnetization curves for Bi_2Se_3 No. 3. (Inset) ^{209}Bi NMR spectra at temperatures of 4.2, 40, and 120 K. The dashed line denotes the reference field for ^{209}Bi at 45.7 MHz.

of conduction electrons, and quadrupolar relaxation ($1/T_{1,q}$) from fluctuations of the electric field gradient, i.e., $1/T_1 = 1/T_{1,m} + 1/T_{1,q}$. The magnetic relaxation by conduction electrons in a semiconductor produces $1/T_{1,m} \propto NT^{0.5}$, which is different from the Korringa relation, $1/T_{1,m} \propto D^2(E_F)T$, for a metal, where N and $D^2(E_F)$, respectively, are the charge carrier concentration and density of states at the Fermi level.[14] In contrast, the quadrupolar relaxation in a semiconductor is independent of the carrier concentration, and is a property of the lattice, so that $1/T_{1,q}$ depends on the details of the phonon spectrum. We are not aware of any universal behavior of the temperature-dependent $1/T_{1,q}$; it should behave differently for temperatures above and below the Debye temperature.[22] Yet, the change in the power law, $1/T_1 \propto T^\alpha$, in Fig. 6, is not related to the Debye temperature, which is ~182 K, beyond our temperature range.[23] The change in power law is most likely due to the competition between the magnetic and quadrupolar relaxations, where the former dominates at low temperature. Therefore the smaller $1/T_1$ at low temperature in sample No. 3, as compared to those in samples Nos. 1 and 2, again suggests that sample No. 3 has a smaller charge-carrier density than the others. In addition, we find a Korringa relation of $1/T_1 \propto T$, for the more conductive samples Nos. 1 and 2, and a power of 0.7, close to the theoretical value of 0.5 for a semiconductor, for the less conductive sample No. 3. This agrees with the resistivity data in Fig. 5, showing metallic- and semiconductor-like behavior in samples Nos. 2 and 3, respectively. The quadrupolar relaxation, which is independent of carrier density, dominates at high temperature, so that the $1/T_1$ curves of all the samples merge at temperatures above 50 K.

Figure 7 shows the magnetization curve for sample No. 3, indicating a diamagnetic material, although with a slight temperature dependence at low temperature. We note that previous studies reported temperature-independent diamagnetism in Bi_2Se_3.[21,24] As the increasing magnetization at low temperature often points to the presence of magnetic-impurities, we wanted to identify the cause of the weak temperature dependence and to investigate the local magnetism in our low-defect Bi_2Se_3 sample No. 3. We performed the ^{209}Bi NMR measurements at three different temperatures, 4.2, 40, and 120 K (see inset of Fig. 7). The spectra shift to the lower field (a higher positive shift) with decreasing temperature. This confirms that the weak temperature dependence of magnetization is not an impurity effect but is intrinsic. In addition, the change in the NMR shift is due to the Fermi contact of the conduction electrons, which changes gradually with temperature. Therefore, we conclude that the weak temperature-dependent magnetization is caused by the slight change of the Pauli susceptibility at low temperature and that the orbital diamagnetism remains temperature independent. As we do not see any surface effects in our NMR spectra, we stress that the observed magnetization is not related to the spin polarization of the topological surface state.[4,25]

IV. CONCLUSIONS

In summary, three Bi_2Se_3 single crystals synthesized by three different methods were characterized by ^{209}Bi NMR. The spectra show intensity anomalies due to the short T_2 effect. The ^{209}Bi NMR signal is entirely from the bulk states, with no detectable contribution from the topological surface state. The NMR linewidth suggests that the structural defect level is different in these differently grown crystals. The Se-rich self-flux growth produces the highest quality single crystal, while the chemical vapor transport and traveling solvent zone growth produce samples of similar, but reduced quality. As Se vacancies necessarily introduce n-type charge carries in Bi_2Se_3, we identify their different concentration as the most probable cause of the observed electronic differences in the ^{209}Bi NMR frequency shift and $1/T_1$. The magnetism in Bi_2Se_3 is diamagnetic, but with a weak temperature dependence at low temperature, caused by the slight temperature-dependent Pauli paramagnetism.

ACKNOWLEDGMENTS

We thank D. E. MacLaughlin for enlightening discussion and Kenneth M. Sasaki for suggesting improvements to the grammar and phrasing of this work. This work is supported by NSC 98-2112-M-009-016-MY3 and the MOE ATU Program. The work at BNL is supported by the Office of Science and US Department of Energy under contract No. DE-AC02-98CH10886.

*Corresponding author: blyoung@mail.nctu.edu.tw

[1] H. Scherrer and S. Scherrer, in *Handbook of Thermoelectrics*, edited by D. M. Rowe (CRC Press, New York, 1994), pp. 211–237.

[2] Y. Xia, D. Qian, D. Hsieh, L. Wray, A. Pal, H. Lin, A. Bansil, D. Grauer, Y. S. Hor, R. J. Cava, and M. Z. Hasan, Nat. Phys. **5**, 398 (2009).

[3]Y. L. Chen, J. G. Analytis, J.-H. Chu, Z. K. Liu, S.-K. Mo, X. L. Qi, H. J. Zhang, D. H. Lu, X. Dai, Z. Fang, S. C. Zhang, I. R. Fisher, Z. Hussain, and Z.-X. Shen, Science **325**, 178 (2009).

[4]D. Hsieh, Y. Xia, D. Qian, L. Wray, J. H. Dil, F. Meier, J. Osterwalder, L. Patthey, J. G. Checkelsky, N. P. Ong, A. V. Fedorov, H. Lin, A. Bansil, D. Grauer, Y. S. Hor, R. J. Cava, and M. Z. Hasan, Nature (London) **460**, 1101 (2009).

[5]X.-L. Qi, R. Li, J. Zang, and S.-C. Zhang, Science **323**, 1184 (2009).

[6]L. Fu and C. L. Kane, Phys. Rev. Lett. **100**, 096407 (2008).

[7]X.-L. Qi, T. L. Hughes, and S.-C. Zhang, Phys. Rev. B **78**, 195424 (2008).

[8]G. Hyde, H. Beale, I. Spain, and J. Woollam, J. Phys. Chem. Solids **35**, 1719 (1974).

[9]Y. S. Hor, A. Richardella, P. Roushan, Y. Xia, J. G. Checkelsky, A. Yazdani, M. Z. Hasan, N. P. Ong, and R. J. Cava, Phys. Rev. B **79**, 195208 (2009).

[10]S.-Y. Xu, Y. Xia, L. A. Wray, S. Jia, F. Meier, J. H. Dil, J. Osterwalder, B. Slomski, A. Bansil, H. Lin, R. J. Cava, and M. Z. Hasan, Science **332**, 560 (2011).

[11]W. G. Clark, M. E. Hanson, F. Lefloch, and P. Ségransan, Rev. Sci. Instrum. **66**, 2453 (1995).

[12]X. Zhu, L. Santos, R. Sankar, S. Chikara, C. Howard, F. C. Chou, C. Chamon, and M. El-Batanouny, Phys. Rev. Lett. **107**, 186102 (2011).

[13]R. W. G. Wyckoff, *Crystal Structures* (Krieger, Malabar, FL, 1986).

[14]A. Abragam, *The Principles of Nuclear Magnetism* (Oxford University Press, Oxford, 1996).

[15]B. F. Williams and R. R. Hewitt, Phys. Rev. **146**, 286 (1966).

[16]H. Hamaed, M. W. Laschuk, V. V. Terskikh, and R. W. Schurko, J. Am. Chem. Soc. **131**, 8271 (2009).

[17]H. Abe, H. Yasuoka, and A. Hirai, J. Phys. Soc. Jpn. **21**, 77 (1966).

[18]G. Miller and C.-Y. Li, J. Phys. Chem. Solids **26**, 173 (1965).

[19]C. P. Slichter, *Principles of Magnetic Resonance* (Springer, New York, 1996).

[20]G. C. Carter, L. H. Bennett, and D. J. Kahan, Prog. Mater. Sci. **20**, 1 (1977).

[21]P. Janíček, Č. Drašar, P. Lošt'ák, J. Vejpravová, and V. Sechovský, Physica B **403**, 3553 (2008).

[22]F. Bridges and W. G. Clark, Phys. Rev. **164**, 288 (1967).

[23]G. E. Shoemake, J. A. Rayne, and R. W. Ure, Phys. Rev. **185**, 1046 (1969).

[24]V. A. Kul'bachinskii, A. Y. Kaminskii, K. Kindo, Y. Narumi, K. Suga, P. Lostak, and P. Svanda, JETP Lett. **73**, 352 (2001).

[25]Z.-H. Pan, E. Vescovo, A. V. Fedorov, D. Gardner, Y. S. Lee, S. Chu, G. D. Gu, and T. Valla, Phys. Rev. Lett. **106**, 257004 (2011).